# The Ig cell adhesion molecule Basigin controls compartmentalization and vesicle release at *Drosophila melanogaster* synapses

Florence Besse,[1] Sara Mertel,[2,3] Robert J. Kittel,[2,3] Carolin Wichmann,[2,3] Tobias M. Rasse,[2,4] Stephan J. Sigrist,[2,3] and Anne Ephrussi[1]

[1]Developmental Biology Unit, European Molecular Biology Laboratory, D-69117 Heidelberg, Germany
[2]European Neuroscience Institute Göttingen, D-37077 Göttingen, Germany
[3]Institut für Klinische Neurobiologie und Rudolf-Virchow-Zentrum, Universität Würzburg, D-97078 Würzburg, Germany
[4]Hertie-Institute for Clinical Brain Research, University of Tübingen, D-72076 Tübingen, Germany

Synapses can undergo rapid changes in size as well as in their vesicle release function during both plasticity processes and development. This fundamental property of neuronal cells requires the coordinated rearrangement of synaptic membranes and their associated cytoskeleton, yet remarkably little is known of how this coupling is achieved. In a GFP exon-trap screen, we identified *Drosophila melanogaster* Basigin (Bsg) as an immunoglobulin domain-containing transmembrane protein accumulating at periactive zones of neuromuscular junctions. Bsg is required pre- and postsynaptically to restrict synaptic bouton size, its juxtamembrane cytoplasmic residues being important for that function. Bsg controls different aspects of synaptic structure, including distribution of synaptic vesicles and organization of the presynaptic cortical actin cytoskeleton. Strikingly, *bsg* function is also required specifically within the presynaptic terminal to inhibit nonsynchronized evoked vesicle release. We thus propose that Bsg is part of a transsynaptic complex regulating synaptic compartmentalization and strength, and coordinating plasma membrane and cortical organization.

## Introduction

Synapses are highly specialized and asymmetric intercellular junctions organized into morphologically, biochemically, and physiologically distinct subdomains. At the presynaptic terminal membrane, active zones mediate $Ca^{2+}$-dependent synaptic vesicle fusion, whereas the surrounding periactive zones are essential for synaptic vesicle endocytosis and the control of synaptic terminal growth (Sone et al., 2000; Zhai and Bellen, 2004). Definition of distinct synaptic subdomains is not restricted to the plasma membrane but is also clearly visible within the presynaptic terminal cytoplasm. Notably, synaptic vesicles are clustered at the cell cortex, in the vicinity of active zones. In addition, they seem organized into functional subpools displaying distinct release and recycling properties (Rizzoli and Betz, 2005). Such an organization requires the precise trafficking and targeting of vesicles to their appropriate location and the specific recruitment and release of subsets of vesicles, depending on the stimulation conditions. One of the main challenges synapses have to face is maintaining such a highly organized structure while constantly adapting their morphology and strength in response to developmental programs and/or external stimuli. Indeed, synaptic terminals can adjust their size; the number, size, and composition of their pre- and postsynaptic membrane specializations; and the availability and release competence of cytoplasmic synaptic vesicles. These dynamic changes require the maintenance of precise physical and functional connections between pre- and postsynaptic compartments, as well as between cytoplasmic and plasma membrane subdomains.

To date, the mechanisms allowing such a dynamic reorganization are still poorly understood. However, using the *Drosophila melanogaster* neuromuscular junction (NMJ) as a genetic model, different components of periactive zones, including transmembrane proteins and adaptor molecules, have been implicated in the control of terminal outgrowth (Schuster et al., 1996b; Beumer et al., 1999; Sone et al., 2000; Koh et al., 2004; Marie et al., 2004). Cell adhesion molecules (CAMs) of the Ig superfamily seem particularly important in maintaining

Correspondence to Stephan J. Sigrist: stephan.sigrist@virchow.uni-wuerzburg.de; or Anne Ephrussi: ephrussi@embl.de

Abbreviations used in this paper: BRP, Bruchpilot; CAM, cell adhesion molecule; CSP, cysteine string protein; eEJC, nerve-evoked excitatory junctional current; NMJ, neuromuscular junction; PSD, postsynaptic density; SSR, subsynaptic reticulum.

The online version of this article contains supplemental material.


The Journal of Cell Biology, Vol. 177, No. 5, June 04, 2007 843–855
http://www.jcb.org/cgi/doi/10.1083/jcb.200701111

the integrity of synaptic terminals but also in transmitting signals to the cell interior, thereby promoting differentiation of pre- and postsynaptic specializations and regulating synaptic structure and function (Schuster et al., 1996a; Stewart et al., 1996; Sone et al., 2000; Polo-Parada et al., 2001; Rougon and Hobert, 2003; Yamagata et al., 2003). Moreover, the actin-rich presynaptic cytoskeleton is important for rearranging synaptic domains and for controlling synaptic vesicle distribution and release ability (Dillon and Goda, 2005). How the linkage between cortical cytoskeleton, cytoplasmic vesicle pools, and specialized membrane domains is mediated and, more generally, how plasma membrane and cytoplasmic membranes are spatially and functionally connected largely remain to be elucidated.

Here, we identify the transmembrane Ig CAM Basigin (Bsg) as a new component of periactive zones at *D. melanogaster* NMJ synapses. Bsg is the only *D. melanogaster* member of the Basigin/Embigin/Neuroplastin family of glycoproteins, of which mammalian Bsg has been shown to have multiple functions, including in tumor progression (Nabeshima et al., 2006). It seems to regulate cell architecture and cell–cell recognition (Fadool and Linser, 1993; Curtin et al., 2005), act in signaling (Guo et al., 1997; Tang et al., 2006), and act as a chaperone for transmembrane proteins (Kirk et al., 2000; Zhou et al., 2005). By analogy to other mammalian cell surface glycoproteins, and in particular to the CD44 transmembrane protein family (Ponta et al., 2003), Bsg may be essential for establishment of transmembrane complexes and for organization of cell structure and signal transduction cascades. Interestingly, mammalian Bsg and Neuroplastin have been suggested to play a role in memory functions and long-term potentiation, respectively, although their precise function has not been determined (Naruhashi et al., 1997; Smalla et al., 2000).

Our in vivo study shows that *D. melanogaster* Bsg is required in both pre- and postsynaptic compartments to control formation and growth of synaptic varicosities (or boutons) at larval NMJs. We also show that Bsg is a bona fide Ig CAM because (1) it can promote cell–cell adhesion and (2) its transmembrane and/or juxtamembrane cytoplasmic domains are critical for its function in vivo. Furthermore, down-regulation of *bsg* affects the size of postsynaptic receptor fields, as well as the distribution of synaptic vesicles within neuronal terminals. These defects are associated with alterations of the actin/Spectrin network, suggesting that Bsg accumulation at the plasma membrane regulates synaptic compartmentalization and architecture. Strikingly, we found that Bsg function is also essential within the presynaptic compartment for the restriction of neurotransmitter release. Based on our in vivo data, we propose that Bsg may be part of a transsynaptic complex surrounding active zones and involved in the coordinated development of pre- and postsynaptic membranes, as well as in the functional coupling of plasma membrane and cortical subdomains.

## Results

### Basigin accumulates at *D. melanogaster* NMJs

To identify new proteins controlling synapse development, we searched for proteins specifically accumulating at developing NMJs of *D. melanogaster* larvae. We performed a protein-trap screen in which GFP fusion proteins expressed from their endogenous promoters are randomly generated (Morin et al., 2001) and screened the expression pattern of ~350 $GFP^+$ lines (see Materials and methods). Thereby, we identified 10 lines exhibiting GFP expression at the larval NMJ and focused on three independent lines showing strong GFP accumulation at larval NMJs, but only low GFP levels along the motoneuron axons, and at the surface of muscle fibers (Fig. 1, A and A′). In these lines, a strong GFP signal is also observed in different neuropil structures of the larval brain (Fig. 1 B).

Using inverse PCR, we found that in each of these three lines the protein-trap cassette was inserted in the gene CG31605, encoding the *D. melanogaster* homologue of the mammalian protein CD147/EMMPRIN/Basigin, Basigin (Bsg; Curtin et al., 2005). According to predictions, the artificial GFP exon should be incorporated upon splicing into mature transcripts whose transcription starts upstream of the insertion, resulting in the in-frame incorporation of GFP. We confirmed this by RT-PCR

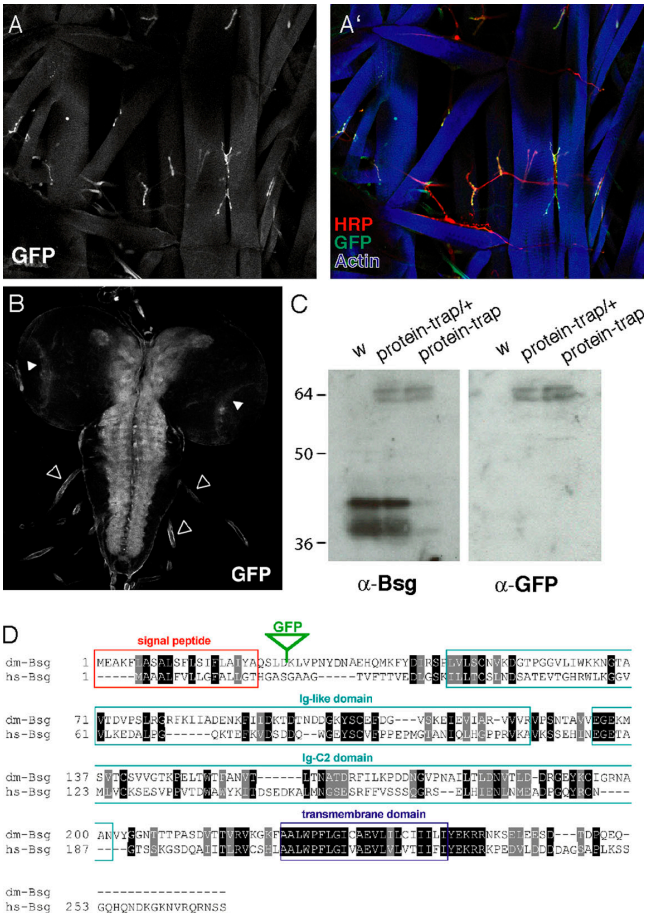


Figure 1. **GFP expression pattern in *bsg* protein-trap lines.** (A and A′) Third instar larva heterozygous for the protein-trap insertion, stained with anti-GFP antibodies (A and A′, green), anti-HRP antibodies (A′, red), and phalloidin (A′, blue). (B) GFP-Bsg accumulation in heterozygous larval brain. (C) Western blot of total extracts from *w* larvae (left) or larvae heterozygous (protein-trap/+; middle) or homozygous (protein-trap; right) for a protein-trap insertion, probed with anti-Bsg and anti-GFP antibodies. (D) Alignment of *D. melanogaster* and human Bsg proteins. The green triangle indicates the location of GFP insertion.

(unpublished data) and Western blot analysis using anti-Bsg antibodies raised against the *D. melanogaster* protein (Fig. 1 C).

*D. melanogaster* Bsg is a small transmembrane protein composed of two extracellular Ig-like domains, a highly conserved transmembrane domain, and a short cytoplasmic tail (Fig. 1 D). Mammalian Basigin has been described as a multifunctional protein regulating different processes, including tumor invasion, reproduction, and sensory and memory functions (Muramatsu and Miyauchi, 2003; Toole, 2003). Interestingly, *bsg* is highly expressed in the mouse nervous system (Fan et al., 1998), and Bsg protein is present in purified postsynaptic densities (PSDs) of mouse central nervous system synapses (Collins et al., 2006). In *D. melanogaster*, Bsg has been proposed to regulate cellular architecture during eye morphogenesis (Curtin et al., 2005). The cellular mechanisms underlying its functions, however, are still poorly understood. Bsg is the only *D. melanogaster* member of a mammalian protein family including Basigin, Embigin, and Neuroplastin/gp65/gp55. All the members of this family have been suggested to regulate cell–substratum adhesion and/or cell–cell adhesion, and are therefore proposed to belong to the Ig CAM family (Fadool and Linser, 1993; Huang et al., 1993; Kasinrerk et al., 1999; Smalla et al., 2000).

## Basigin accumulates at periactive zones

To check if the distribution of tagged Bsg reflects that of the endogenous protein, we stained wild-type larvae with anti-Bsg antibodies. Endogenous Bsg shows a localization pattern identical to that of the GFP fusion (Fig. 2 A), and both precisely colocalize with Discs large (Dlg), a transmembrane protein present both pre- and postsynaptically, but mainly accumulating in stacks of postsynaptic membranes named subsynaptic reticulum (SSR; Fig. 2, A″ and B″; Lahey et al., 1994). Like Dlg, Bsg accumulates to higher levels at type $I_b$ than at smaller type $I_s$ boutons (Fig. 2, A and B; and not depicted). To exclusively visualize the presynaptic expression of Bsg, we next expressed a GFP-tagged Bsg fusion specifically in the presynaptic compartment (Fig. 2 C) and observed a robust GFP signal at NMJs. Consistent with an accumulation of Bsg at the presynaptic membrane, the inner aspect of both endogenous Bsg and GFP-Bsg protein-trap fusion labels partially overlap with the presynaptic membrane marker HRP (Fig. 2, D and E).

Further analysis revealed that Bsg is not homogenously distributed at the membrane but is excluded from active zones labeled with anti-Bruchpilot (BRP) NC82 antibodies (Fig. 2 F; Wagh et al., 2006). Therefore, similar to other transmembrane proteins involved in the structural control of synaptic terminals, such as Dlg or Fasciclin II (Fas II), Bsg localizes to periactive zones (Sone et al., 2000).

## Identification of *basigin* mutants

According to data from the *D. melanogaster* genome project, *bsg* encodes nine distinct putative transcripts, of which eight encode the same protein (Fig. 3 A). One of the predicted transcripts, RG, encodes a slightly different protein. However, this transcript is barely detected after quantitative RT-PCR on larval fillet extracts (unpublished data).

To address the in vivo requirement for Bsg at the larval NMJ, we searched for *P* element insertions near the transcription starts of the longer transcripts and found five belonging to the same lethal complementation group. Three of these (l[2]k13638, l[2]k14308, and NP3198), when placed in trans over a deficiency covering the locus (*Df[2L]Exel7034*, hereafter referred to as *Df*), cause an embryonic/early larval lethality that can be rescued by ubiquitous expression of a *bsg* transgene (Fig. 3 B), and represent strong hypomorphic alleles (Curtin et al., 2005; unpublished data). Two other insertions, NP6293 and l(2)SH1217, behave genetically as weaker hypomorphic alleles, as, respectively, 30 and 50% of the corresponding hemizygotes

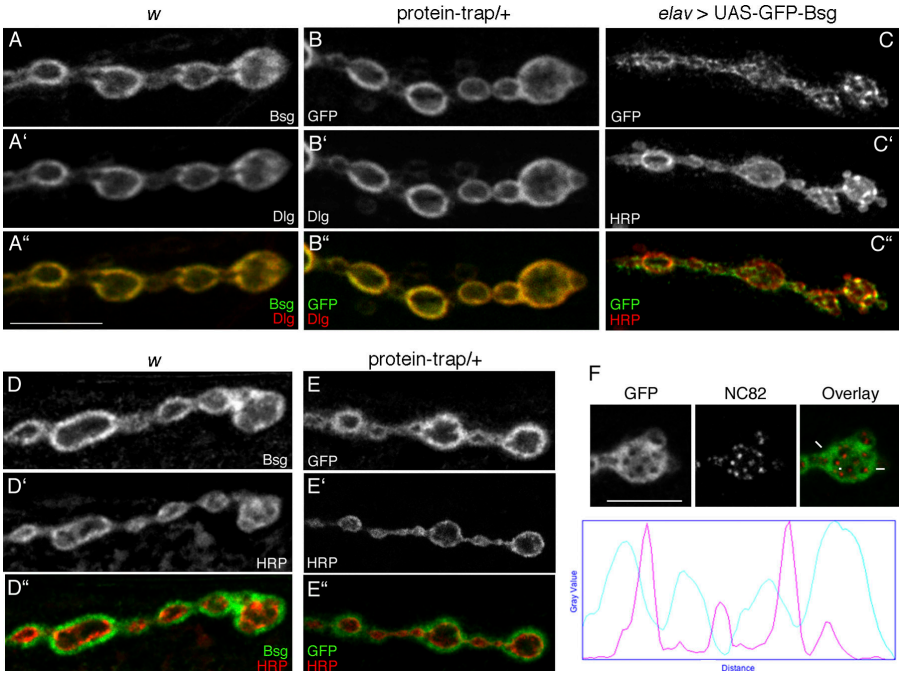


Figure 2. **Bsg accumulation at the NMJ.** (A and B) NMJs of *w* (A) or protein-trap/+ (B) larvae double stained with anti-Bsg (A) or anti-GFP (B) antibodies and anti-Dlg antibodies (A′ and B′). (C) *elav*-Gal4/+; UAS-GFP-*bsg*/+ larvae stained with anti-GFP (C) and anti-HRP (C′) antibodies. (D and E) NMJs of *w* (D) and protein-trap/+ (E) larvae double stained with anti-Bsg (D) or anti-GFP (E) and anti-HRP (D′ and E′) antibodies. A–E correspond to z projections of serial confocal sections. Bar, 10 µm. (F) Tangential confocal section of a protein-trap/+ synaptic bouton stained with anti-GFP and NC82 anti-BRP antibodies and plot of the intensity profiles of GFP (green) and NC82 (pink) stainings across the bouton (section is indicated by white marks on the overlay). A–E are from muscle 6/7 NMJs, and F is from muscle 4 NMJ. Bar, 5 µm.

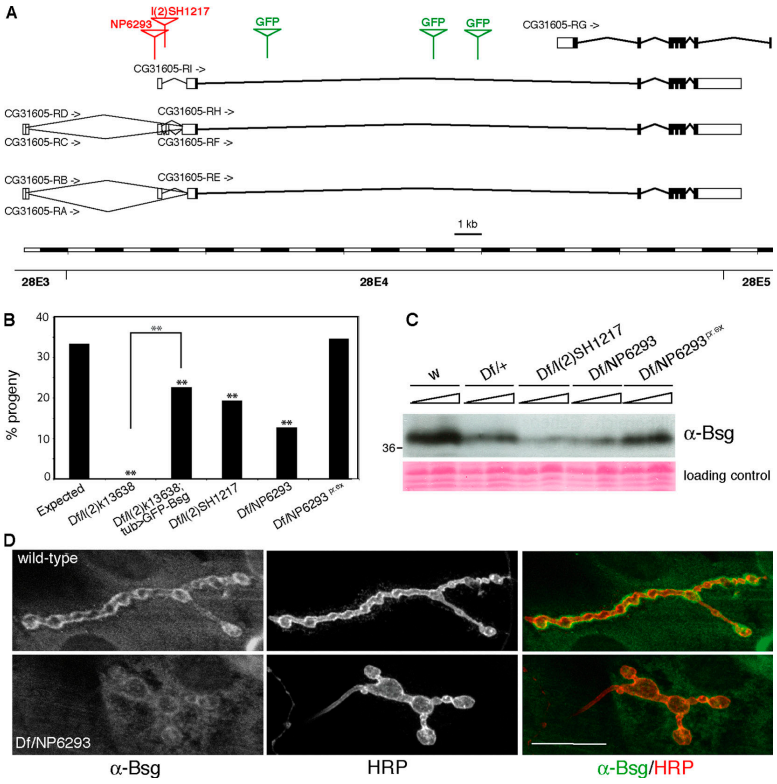


Figure 3. ***bsg* locus and mutants.** (A) Genomic organization and intron–exon structure of *bsg*. Untranslated and coding regions are represented as white and black boxes, respectively. Positions of *P* element and GFP-containing *piggyBac* insertions are indicated in red and green, respectively. (B) Percentages of GFP$^-$ third instar larvae recovered among the progeny of a cross between *Df*/CyO-GFP females and l(2)k13638/CyO-GFP, l(2)SH1217/CyO-GFP, NP6293/CyO-GFP, or NP6293$^{pr.ex}$/CyO-GFP males. 33% of GFP$^-$ animals are expected in absence of lethality. NP6293$^{pr.ex}$ is the NP6293 chromosome obtained after precise excision of the *P* element. The third bar corresponds to rescued *Df*/l(2)k13638; UAS-GFP-Bsg-fl/*tub*-Gal4 larvae. Note that ~80% (16/20) of these larvae developed into pharate adults, of which 38% (6/16) hatched. At least 177 larvae were scored per cross. Statistical comparisons to the "expected" control: **, $P < 0.001$ ($\chi$ test). (C) Western blot of wild-type and mutant body wall extracts, probed with anti-Bsg antibodies. Ponceau staining is shown as a loading control. (D) Wild-type (top) and *Df*/NP6293 (bottom) larvae stained with anti-Bsg and anti-HRP antibodies. It was necessary to use diluted and purified anti-Bsg serum to visualize the difference in expression levels. Both pictures were taken from muscle 4 NMJs using identical confocal settings. Bar, 20 μm.

reach third larval instar (Fig. 3 B). This semilethality is reverted after precise excision of NP6293 (Fig. 3 B). Consistent with these data, Western blot analysis shows that Bsg expression levels are greatly reduced in *Df*/NP6293 and *Df*/l(2)SH1217 mutant larvae but restored to normal levels after precise excision of NP6293 (Fig. 3 C). The amount of Bsg specifically accumulating at the NMJ is also significantly reduced in *Df*/NP6293 larval fillets, compared with wild type (Fig. 3 D). Together, these results show that NP6293 and l(2)SH1217 are *bsg* mutant alleles suitable for analysis of larval NMJ development and maturation. We therefore renamed them $bsg^{6293}$ and $bsg^{1217}$ and used them for subsequent studies.

## Basigin is required in both pre- and postsynaptic compartments to restrict bouton size and allow efficient NMJ expansion

To determine whether *bsg* mutants exhibit defects in their motoneuron connection pattern and/or NMJ morphology, we examined synaptic boutons and motoneuron membranes of both $Df/bsg^{6293}$ and $Df/bsg^{1217}$ third instar larvae. Axonal targeting is not altered to a visible degree in these animals. However, the growth of synaptic boutons is strongly altered, as revealed by the considerable increase in their size (Fig. 4, C–G; and Table S1, available at http://www.jcb.org/cgi/content/full/jcb.200701111/DC1). In particular, the proportion of very large boutons (>12 μm$^2$) is greatly increased in *bsg* mutants compared with controls (Fig. 4 G and Table S1; $P < 0.001$). The observed increase in bouton size is associated with a concomitant reduction of both NMJ branching and bouton number (Fig. 4, C–F and H; and Table S1), keeping the overall NMJ size close to normal (muscle 4 NMJ area: 165.33 ± 9 μm$^2$ [$n$ = 18] and 163.97 ± 15 μm$^2$ [$n$ = 12] for $Df/bsg^{6293}$ and *w* larvae, respectively; $P > 0.05$). Moreover, defects in bouton size and number are already observed in second instar animals (Fig. S1) and revert after precise excision of NP6293 (Fig. 4 H and Table S1).

To explicitly determine whether these growth defects could be rescued and whether they reflected pre- and/or postsynaptic function of *bsg* at the NMJ, we expressed a wild-type copy of *bsg* in specific compartments of $Df/bsg^{6293}$ larvae. Expression of wild-type Bsg solely in muscles (using *mhc*-Gal4 or 24B-Gal4) or in neurons (using *elav*-Gal4), partially, but significantly, rescued both the increase in bouton size and the reduction of bouton number observed in mutant larvae (Fig. 4, I, J, L, and M; and not depicted). Near-complete rescue of bouton size and junction growth was obtained only when expressing wild-type Bsg both pre- and postsynaptically (Fig. 4, K, L, and M; and Table S1).

Collectively, we conclude that Bsg is needed for efficient outgrowth of larval NMJs and that its function is required in both pre- and postsynaptic compartments to define boutons of proper size. Such a dual requirement is documented for the Ig CAM Fas II and is thought to reflect the establishment of transsynaptic homophilic interactions (Schuster et al., 1996a). We thus tested whether Bsg might also promote cell–cell adhesion. As shown in Fig. 4 N, S2 cells transfected with a GFP-Bsg construct strongly adhere to each other, whereas S2 cells transfected with a control GFP construct do not. Thus, Bsg promotes cell aggregation, consistent with the idea that Bsg could regulate the addition and growth of synaptic boutons through modulation of cell adhesion.

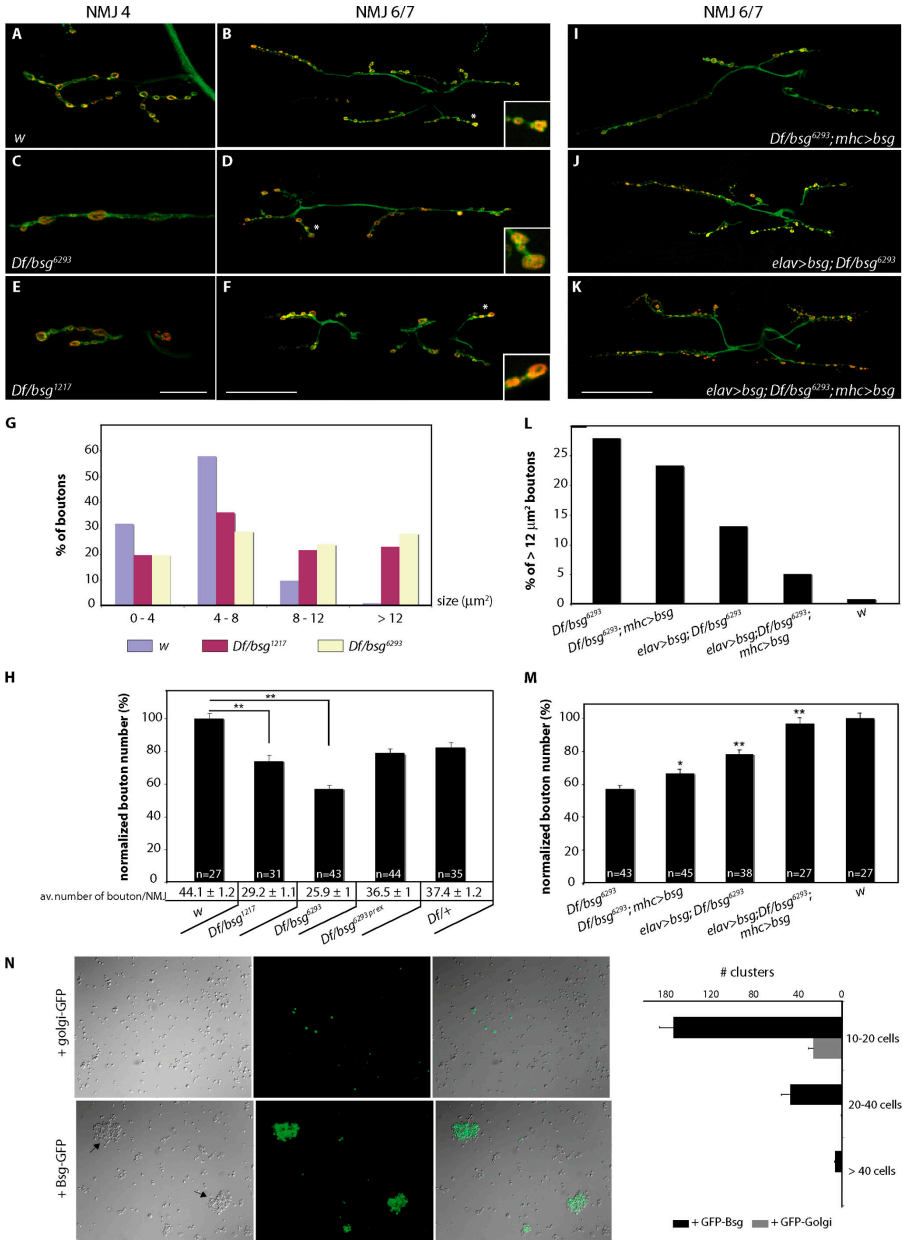


Figure 4. ***bsg* regulates NMJ growth.** (A–F) NMJs at muscle 4 (A, C, and E) or muscles 6/7 (B, D, and F) of *w* (A and B), *Df/bsg*$^{6293}$ (C and D), and *Df/bsg*$^{1217}$ (E and F) larvae stained with anti-CSP (red) and anti-HRP (green) antibodies. Asterisks in B, D, and F mark the branch terminals chosen for magnification (insets). Bars: (A, C, and E) 20 µm; (B, D, and F) 60 µm. (G) Distribution of synaptic boutons according to their size (in µm$^2$). At least 97 boutons were scored per genotype. (H) Quantification of muscle 6/7 type $I_b$ bouton number. Bouton numbers were normalized to muscle surface area, and the reference was set to 100 for *w* control larvae. Note that removal of one copy of *bsg* causes a mild reduction of bouton number, indicating a dosage sensitivity of the phenotype. Because of the smaller muscle size of *Df/bsg*$^{1217}$ larvae, their bouton number is increased artificially upon normalization (numerical values below the bars represent the raw data, which are also shown in Table S1, available at http://www.jcb.org/cgi/content/full/jcb.200701111/DC1). Statistical comparisons to the *w* controls: **, $P < 0.001$ (*t* test). *n* represents the number of junctions scored per genotype. Error bars indicate SEM. (I–K) NMJs at muscle 6/7 of *Df/bsg*$^{6293}$; *mhc*-Gal4/UAS-*bsg* (I), *elav*-Gal4/+; *Df/bsg*$^{6293}$; UAS-*bsg*/+ (J), and *elav*-Gal4/+; *Df/bsg*$^{6293}$; *mhc*-Gal4, UAS-*bsg*/+ (K) larvae double stained with anti-CSP (red) and anti HRP (green) antibodies. Bar, 60 µm. (L) Percentage of synaptic boutons >12 µm$^2$ in *Df/bsg*$^{6293}$ larvae and different rescue contexts. At least 114 boutons were scored per genotype. (M) Quantification of muscle 6/7 type $I_b$ bouton numbers in *Df/bsg*$^{6293}$ larvae and different rescue contexts. Bouton numbers were normalized to muscle surface area, and the reference set to 100 for *w* control larvae. Statistical comparisons to *Df/bsg*$^{6293}$ animals: *, $P < 0.05$; **, $P < 0.001$ (*t* test). *n* represents the numbers of junctions scored per genotype. Error bars indicate SEM. (N) Cell aggregation assays using S2 cells transfected with either a GFP control construct (GFP-Golgi) or GFP-Bsg. (left) Light microscopy pictures; (right) number of clusters containing 10–20 cells, 20–40 cells, or >40 cells (per 5 × 10$^4$ cells). Four samples, from two independent transfections, were analyzed per construct.

## A conserved juxtamembrane basic motif is crucial for Basigin function in vivo

Depending on the cell type and/or the protein partners, different domains of mammalian Bsg are required for its activity (Guo et al., 1997; Kirk et al., 2000; Sun and Hemler, 2001). Thus, to determine which domains of *D. melanogaster* Bsg are required for its function at the larval NMJ, we generated GFP-tagged truncated variants (Fig. 5 A) and assayed their capacity to rescue *Df/bsg*$^{6293}$ morphological defects.

Bsg lacking the most C-terminal part of the intracellular domain (Δintra) rescues defects in bouton size and number similarly to the full-length tagged form (fl) when expressed presynaptically (Fig. 5, D and E). In contrast, forms composed of the two Ig domains only (Extra) or of the two Ig domains of Bsg fused to the transmembrane and intracellular domains of rat CD2 (Bsg-CD2) do not significantly rescue the decrease in bouton number observed in *bsg* mutants and only poorly rescue bouton growth defects (Fig. 5, D and E). Thus, Bsg transmembrane and/or juxtamembrane cytoplasmic domains appear crucial for regulation of NMJ bouton growth and budding by Bsg.

The cytoplasmic juxtamembrane region of Bsg contains a conserved cluster of positively charged residues (KRR; Fig. 5 B). We found that when KRR is substituted with NGG, the mutated protein only poorly rescues the reduced bouton number and only to a low extent the increased bouton size of *bsg* larvae (Fig. 5, D and E). Moreover, ubiquitous expression of the KRR→NGG mutated protein does not significantly rescue the early lethality of the strong mutant combination *Df*/l(2)k13638, whereas full-length Bsg does (Fig. 5 C), further indicating a crucial and previously unknown role of this motif for Bsg function.

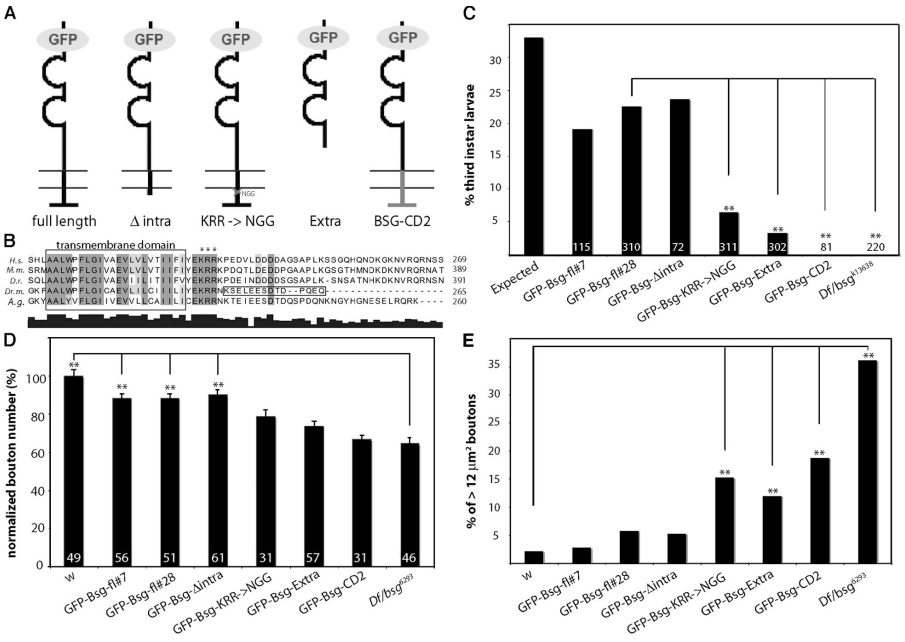


Figure 5. **Differential rescue capacity of various mutated Bsg proteins.** (A) Scheme of Bsg variants. Δintra corresponds to a form lacking the last 14 amino acids but including the juxtamembrane KRR stretch, Extra to a form lacking both the transmembrane and the cytoplasmic domains, KRR→NGG to a full-length protein where the KRR residues have been substituted to NGG, and Bsg-CD2 to a chimeric protein composed of the two Ig domains of Bsg fused to the transmembrane and cytoplasmic domains of rat CD2. (B) Alignment of Bsg transmembrane and intracellular domains. *H.s.*, *Homo sapiens*; *M.m.*, *Mus musculus*; *D.r.*, *Danio rerio*; *Dr. m.*, *D. melanogaster*; *A.g.*, *Anopheles gambiae*. The black box indicates the amino acids deleted in the Δintra construct. (C) Percentages of non–CyO-GFP third instar larvae recovered among the non-TM6 progeny of a cross between *Df*/CyO-GFP; UAS-GFP-Bsg*/TM6 females and l(2)k13638/CyO-GFP; *tub*-Gal4/TM6 males. 33% of non–CyO-GFP animals are expected in case of complete rescue (left bar). Numbers correspond to the total numbers of non-TM6 larvae scored in the entire progeny of each cross. Statistical comparison to GFP-Bsg-fl#28 animals: **, $P < 0.001$ ($\chi$ test). (D) Quantification of muscle 6/7 type $I_b$ bouton numbers in $Df/bsg^{6293}$ larvae and different rescue contexts (driver used for rescue: *elav*-Gal4). Statistical comparisons to $Df/bsg^{6293}$ animals: **, $P < 0.001$ (*t* test). The number of junctions scored for each genotype is represented in white. Error bars indicate SEM. fl#7 and fl#28 represent two independent insertions of the GFP-tagged full-length transgene. (E) Percentage of synaptic boutons >12 $\mu m^2$ in $Df/bsg^{6293}$ larvae and different rescue contexts. Statistical comparison to *w* animals: **, $P < 0.001$ ($\chi$ test).

### The specification of active zones and periactive zones is normal in *basigin* mutants

Given that *bsg* mutants exhibit defective NMJ morphology, we next tested whether the assembly and/or maintenance of pre- and postsynaptic specializations might also be altered. As shown in Fig. S2 (A and B; available at http://www.jcb.org/cgi/content/full/jcb.200701111/DC1), the overall distribution and complementary accumulation of markers specific to perisynaptic zones and PSDs seems to be normal at *bsg* junctions. Moreover, no alteration of SSR integrity could be detected at the light microscopy level (Fig. S2, C and D) or at the ultrastructural level (Fig. 6 E).

Next, we assayed the distribution of receptor fields and active zones, using antibodies recognizing the glutamate receptor subunit GluRIID (Qin et al., 2005) in combination with anti-BRP NC82 antibodies (Wagh et al., 2006). As illustrated in Fig. 6 (A and B), the distribution of these two markers is normal at *bsg* junctions: BRP and GluRIID remain concentrated in individual puncta of normal intensity and distribution (density of $BRP^+$ puncta: $1.35 \pm 0.3/\mu m^2$ and $1.19 \pm 0.2/\mu m^2$ for *w* and $Df/bsg^{6293}$ third instar larvae, respectively; $P > 0.05$). Moreover, as described for wild-type animals, $BRP^+$ release sites are reproducibly found in direct apposition to postsynaptic glutamate receptor clusters in *bsg* larvae (Fig. 6, A and B, insets; and not depicted). Consistent with these observations, transmission EM showed that active zones are found at normal frequency and that their characteristic electron-dense specializations (T-bars) are of normal morphology (Fig. 6, D–I). Quantification, however, indicated a slight increase in the electron-dense PSD diameter (Fig. 6 I), which correlates with a slight, but significant, increase in the mean size of GluRIID clusters observed using light microscopy ($w = 0.76 \pm 0.01$ μm, $n = 525$; $Df/bsg^{6293} = 0.84 \pm 0.01$ μm, $n = 501$; $P < 0.001$; Fig. 6 C). Thus, these results suggest that, although Bsg is involved in definition of receptor field size, its function is not essential for specifying active and periactive zone domains.

### Presynaptic actin cytoskeleton organization is altered in *basigin* boutons

Given that *D. melanogaster* Bsg has been suggested to regulate cell architecture, possibly by modulating the cell cytoskeleton (Curtin et al., 2005), we checked the integrity of the actin-based cytoskeleton at *bsg* NMJs. α-Spectrin (α-Spec) closely associates with the NMJ juxtamembrane actin-rich cytoskeleton (Ruiz-Canada et al., 2004). Although it is mainly enriched in the postsynaptic peribouton area, α-Spec is also found at the inner presynaptic bouton cortex (Fig. 7, A and C1; Pielage et al., 2005). In *bsg* larvae, even though no major alterations of the postsynaptic Spectrin cytoskeleton are observed, α-Spec aggregates are detected within the bouton lumen (Fig. 7, B, D1, and E1) in ∼38% of NMJ branches (Fig. 7 L). These aggregates are ∼0.5 μm large and contain other α-Spec–associated proteins, such as β-and βH-Spectrin (not depicted), as well as the actin-associated protein Wasp (Fig. 7, G and G′). In contrast, no enrichment of microtubule-associated proteins was observed in these aggregates (Fig. 7, I′ and I″). To more directly and specifically visualize the presynaptic F-actin network, we expressed the F-actin–binding domain of Moesin fused to GFP (GFP-GMA) exclusively in neurons (Dutta et al., 2002). As shown in Fig. 7 J, GFP-GMA accumulates at the cortex of wild-type synaptic boutons. In *bsg* mutants, although a cortical actin network is still clearly detected at the periphery of boutons, clusters of F-actin filaments are also

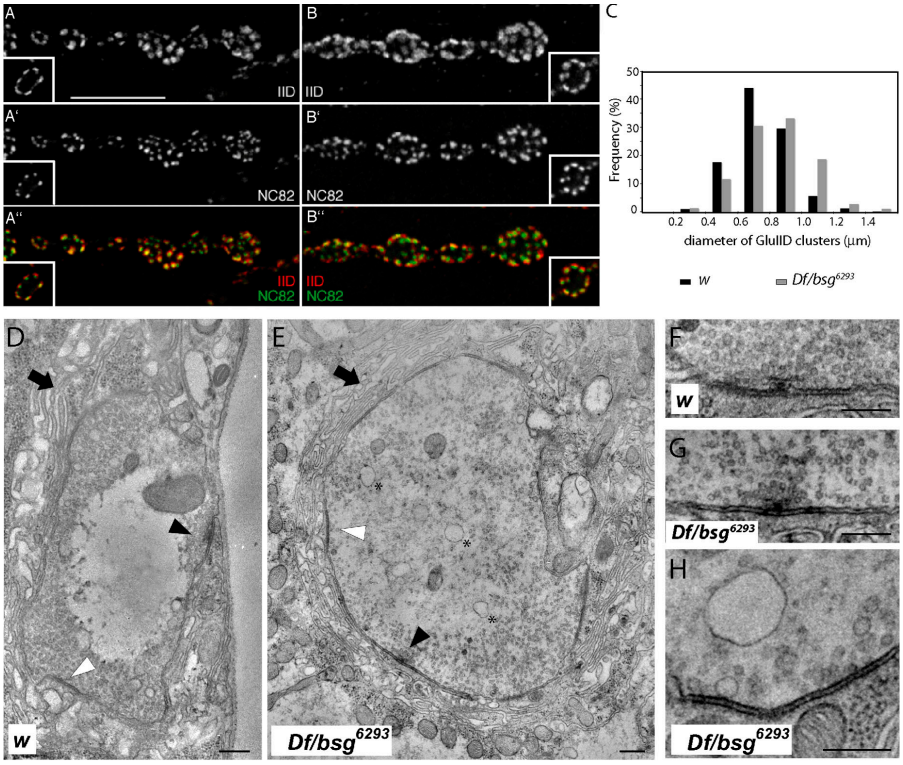


I

| | T-bars | | PSD diameter (n) | |
|---|---|---|---|---|
| | platform diameter (n) | height (n) | | |
| control | 164.3 ± 33.63 nm (10) | 53.14 ± 9.23 nm (17) | 472.01 ± 179.6 nm (39) | p < 0.05 |
| *Df/bsg*$^{6293}$ | 174.2 ± 50.5 nm (11) | 53.16 ± 5.0 nm (13) | 557.5 ± 165.3 nm (44) | |

Figure 6. **Pre- and postsynaptic specializations in *bsg* mutants.** (A and B) *w* (A) and *Df/bsg*$^{6293}$ (B) NMJs stained with anti-GluRIID (A and B) and anti-BRP (A′ and B′) antibodies. Insets show cross-sections of single boutons. Bar, 10 µm. (C) Frequency distribution of postsynaptic glutamate receptor cluster sizes in *w* (black) and *Df/bsg*$^{6293}$ (gray) third instar larvae. (D and E) Electron micrographs of *w* (D) and *Df/bsg*$^{6293}$ (E) type $I_b$ boutons. Arrows point to the SSR, whereas black and white arrowheads indicate active zones, with and without T-bars, respectively. Asterisks indicate atypically large vesicles. Although, in E, synaptic vesicles are also localized in the bouton center, an unambiguous identification of ectopically localized synaptic vesicles was more difficult in other samples. Bars, 250 nm. (F–H) Magnification of *w* (F) and *Df/bsg*$^{6293}$ (G) active zones. (H) Example of an abnormally large vesicle in proximity to a *Df/bsg*$^{6293}$ active zone (defined by its electron-dense plasma membrane and synaptic vesicle cluster). (I) Transmission EM–based quantification of active zone and PSD parameters.

frequently present within them (Fig. 7, K and L). Altogether, these observations indicate that the organization of the presynaptic F-actin network is altered at *bsg* NMJs.

## Diffuse distribution of synaptic vesicles at *basigin* NMJs

In the course of our ultrastructural analysis, we observed that abnormally large vesicles (diameter of up to ∼300 nm) are present in *Df/bsg*$^{6293}$ boutons (Fig. 6, E and H) but are only rarely observed after presynaptic reexpression of Bsg in this background (not depicted). The exact nature of these vesicles remains unclear, as we have not observed any concomitant alteration in the distribution and/or size of the FYVE-GFP$^{+}$ endosomal compartment (Wucherpfennig et al., 2003) at the light microscopy level (unpublished data).

To determine whether these defects could be associated with an alteration of the synaptic vesicle compartment, we analyzed synaptic vesicle distribution using specific vesicle markers. In wild-type boutons, synaptic vesicles are clearly enriched at the cortex but are largely excluded from their central core (Fig. 8, A and A′). In contrast, in *bsg* larvae, preferential association of vesicles with the bouton cortex is lost in ∼60% of NMJ branches (Fig. 8 D), and CSP$^{+}$ (cysteine string protein) vesicles fill parts of (Fig. 8, B–B″) or even the entire lumen (Fig. 8. C–C″) of the bouton. CSP staining is also abnormally strong in axonal tracts connecting boutons and appears more granular than in control animals (Fig. 8, B and C). An essentially identical mislocalization was observed using two other independent markers of synaptic vesicles, Synaptotagmin and Synapsin (Fig. 8, E–H). These defects do not indirectly result from the increase in bouton size observed in *bsg* mutants, as synaptic vesicle localization appears normal in *fas*$^{e76}$ hemizygous larvae, which also form abnormally large boutons (Schuster et al., 1996a; Stewart et al., 1996; unpublished data). Together with the fact that such a diffuse distribution can be observed upon tracking of freshly endocytosed synaptic vesicles (FM 1–43 loading assay; Fig. S3, C and D, available at http://www.jcb.org/cgi/content/full/jcb.200701111/DC1), our data suggest that Bsg specifically regulates the spatial distribution of synaptic vesicles and, in particular, their proper anchoring to the cortex of synaptic boutons.

## Presynaptic down-regulation of Basigin causes excessive, atypically delayed vesicle release

To address whether the observed changes in the distribution of synaptic vesicles might be linked to functional changes in transmitter release, we recorded postsynaptic currents at larval NMJs. As shown in Fig. 9 A, the amplitude of the postsynaptic response to the fusion of single vesicles (minis) is increased above wild-type levels in *bsg* mutants (Fig. 9 A, bottom right; Fig. S3 B; and Table S2, available at http://www.jcb.org/cgi/content/full/jcb.200701111/DC1). This effect is most likely related to the observed enlargement of the postsynaptic glutamate receptor clusters (Fig. 6 C), given that no increase in the size of

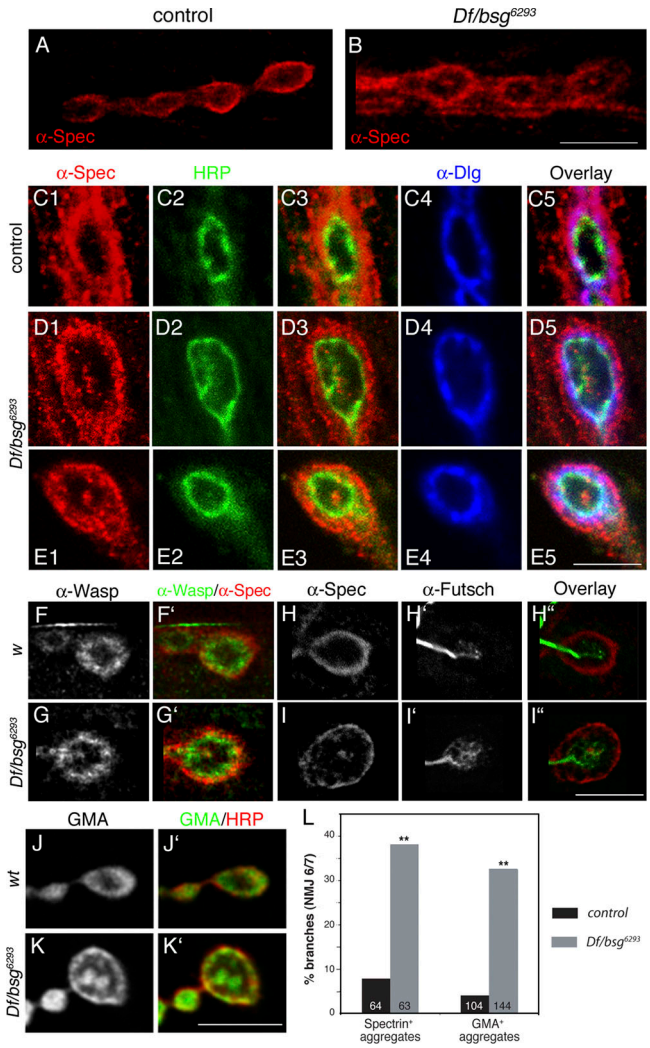


Figure 7. **Distribution of actin cytoskeleton markers is altered in *bsg* larvae.** (A and B) Wild-type (A) and *Df/bsg*$^{6293}$ (B) muscle 4 NMJs stained with anti–α-Spec antibodies. Bar, 10 μm. (C–E) Heterozygous control (C) and *Df/bsg*$^{6293}$ (D and E) boutons stained with anti–α-Spec (C1, D1, and E1), anti-HRP (C2, D2, and E2), and anti-Dlg (C4, D4, and E4) antibodies. Bar, 5 μm. (F and G) *w* (F) and *Df/bsg*$^{1217}$ (G) bouton stained with anti-Wasp (F and G) and anti–α-Spec (F′ and G′, red) antibodies. (H and I) *w* (H) and Df/*bsg*$^{6293}$ (I) boutons stained with anti–α-Spec (H and I) and anti-Fusch (H′ and I′) antibodies. Bar, 5 μm. (J and K) Synaptic boutons of wild-type (J) and *Df/bsg*$^{6293}$ (K) larvae expressing a fusion of GFP with the F-actin binding domain of Moesin (GMA), under the control of *elav*-Gal4. GFP-GMA expression is shown in J and K, and is in green in J′ and K′. HRP staining is shown in red in J′ and K′. Bar, 5 μm. Images A and B correspond to z projections of serial confocal sections throughout entire boutons (step size: 0.3 μm), and images C–K correspond to single optical slices taken through bouton centers. (L) Graph showing the percentage of NMJ 6/7 branches containing presynaptic Spec$^{+}$ or GMA$^{+}$ aggregates. **, $P < 0.001$ ($\chi$ test).

synaptic vesicles was found in *bsg* mutants compared with *w* controls (*Df/bsg*$^{6293}$, 34.4 ± 6.6 nm; *w*, 34.8 ± 7.2 nm; $P > 0.5$). Notably, the frequency of spontaneous release events is strongly elevated in *bsg* mutants (Fig. 9 A, bottom left), and these events often occur clustered in "exocytotic bursts" (Fig. 9 A, asterisk).

The mean amplitude of nerve-evoked excitatory junctional currents (eEJCs) is also increased at *bsg* NMJs (Fig. 9 B), which largely correlates with the observed enlargement of minis (Table S2). However, the temporal profile of *bsg* mutant eEJCs is strikingly lengthened, reflecting a dramatic and atypically delayed release of vesicles. Indeed, although the charge carried by *bsg* mutant minis is only moderately increased (1.5-fold increase; Table S2), a near eightfold elevation of the charge transferred to the postsynapse after exocytosis occurs upon initial nerve stimulation (Fig. 9 C and Table S2). Notably, this value decreases progressively after further low-frequency stimulation, which may result from the exhaustion of the abnormally recruited pool of vesicles responsible for the atypically delayed release component. Averaging the charge transferred over 15 consecutive sweeps nonetheless reveals a near fivefold increase in *bsg* mutants (Table S2); therefore, a more than threefold elevation of the number of vesicles released per action potential (quantal content) is estimated to occur.

These defects reflect a requirement for Bsg within the presynaptic terminal, as sole presynaptic expression of wild-type Bsg in the mutant background rescues both the asynchronous evoked release (Fig. 9 B) and the high frequency of spontaneous release (Fig. 9 A, bottom left), whereas its sole postsynaptic reexpression does not (Fig. 9, A–C). Interestingly, the presynaptic reexpression of Bsg even decreases the amplitude of eEJCs and the frequency of minis below control levels, indicating a dose-dependent role of presynaptic Bsg in restricting vesicle release.

## Discussion

In this study, we have identified the small transmembrane Ig CAM Bsg as a new component of perisynapti c zones of *D. melanogaster* NMJs. We have shown that Bsg function is required in pre- and postsynaptic compartments for the formation and growth of synaptic boutons and that Bsg controls different aspects of synapse structure, including distribution of synaptic vesicles and organization of the presynaptic terminal cortical actin network. Bsg behaves as a canonical Ig CAM, as it promotes cell–cell adhesion and has a conserved motif in its cytoplasmic tail essential for its function in vivo. We propose that Bsg is part of a transsynaptic complex regulating synaptic growth and structural organization. Moreover, and very originally for an Ig CAM, we found that Bsg is essential for inhibiting transmitter release and that this function is restricted to the presynaptic compartment.

### Basigin controls synaptic terminal growth and synaptic organization

In *D. melanogaster*, the final pattern of larval motoneuron connections and the establishment of synapses are complete by the end of embryogenesis, yet NMJs are highly dynamic during larval development, expanding through sprouting of new branches and addition of new synaptic boutons (Schuster et al., 1996a). Here, we have shown that down-regulation of Bsg levels at the *D. melanogaster* NMJ strongly affects bouton growth and budding, resulting in a decrease in bouton number. This effect is probably independent of the increased transmitter release observed in *bsg* larvae because (1) it is already observed in early second instar larvae and (2), in contrast to the increased neurotransmission phenotype, it corresponds to a requirement for *bsg*

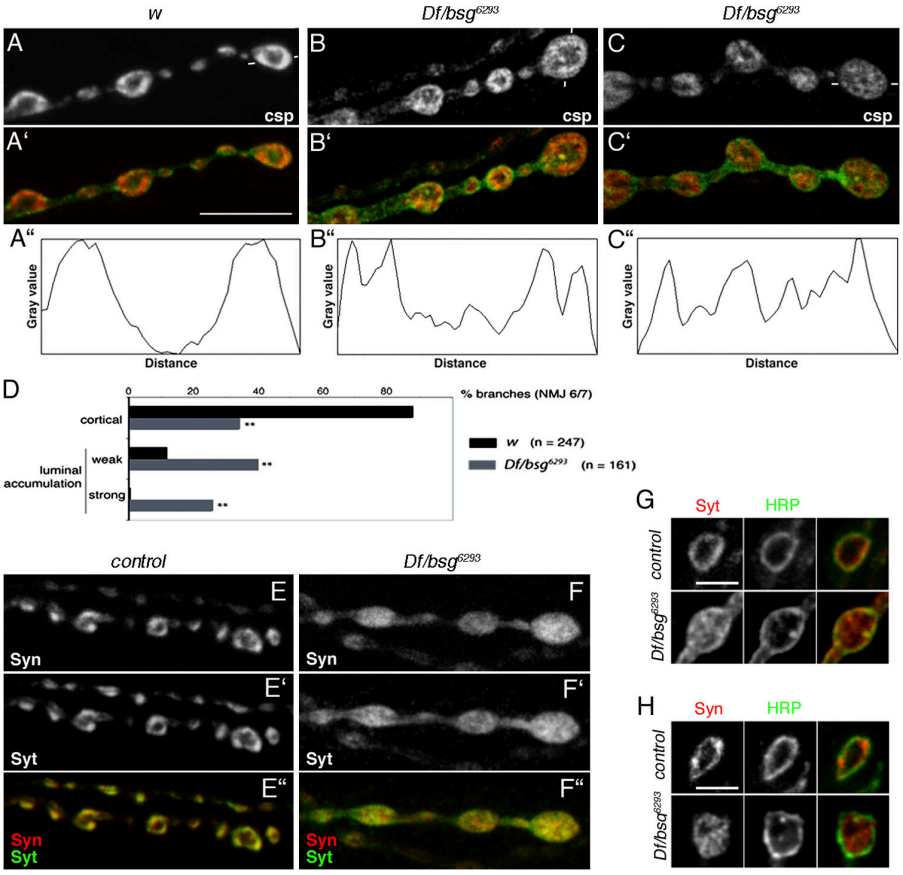


Figure 8. **Synaptic vesicle distribution is altered in *bsg* larvae.** (A–C) *w* (A) and *Df/bsg*$^{6293}$ (B and C) larvae stained with anti-CSP (A–C and A′–C′, red) and anti-HRP antibodies (A′–C′, green). (A″–C″) Fluorescence intensity profiles of CSP staining along a section of the terminal bouton indicated in A–C (white marks). (D) Graph showing the proportion of NMJ 6/7 branches showing either a cortical or luminal accumulation of CSP. **, $P < 0.001$ ($\chi$ test). (E and F) Wild-type (E) and *Df/bsg*$^{6293}$ (F) larvae expressing GFP-tagged synaptotagmin and stained with anti-Synapsin (E and F) and anti-GFP (E′ and F′) antibodies. Images in A–F correspond to z projections of serial confocal sections throughout entire boutons (see Fig. S3 A, available at http://www.jcb.org/cgi/content/full/jcb.200701111/DC1, for serial individual pictures corresponding to pictures E and F). Bar, 10 μm. (G and H) Single confocal sections of *bsg*$^{6293}$/+ and *Df/bsg*$^{6293}$ larvae double stained for Synaptotagmin-GFP (Syt; G) or Synapsin (Syn; H) and HRP. Optical slices all traverse bouton centers (defined by the section with the largest bouton diameter and the ring-like appearance of HRP staining). Bars, 4 μm.

function in both pre- and postsynaptic compartments. This may reflect a role of Bsg in regulating adhesion between pre- and postsynaptic membranes, as described for the Ig CAM Fas II (Schuster et al., 1996a). Bsg function is, however, not restricted to modulation of synaptic membrane adhesiveness, as mutant forms lacking the transmembrane and/or juxtamembrane cytoplasmic domains can promote cell–cell aggregation (Fig. S1 B) but function poorly in vivo. Bsg may thus also signal toward the cell cytoplasm and/or regulate the actin cytoskeleton (see the following section).

In addition, Bsg controls synaptic architecture: it modulates the size of postsynaptic glutamate receptor fields and, more strikingly, is required for the anchoring of synaptic vesicles to the presynaptic terminal cortex. This suggests that Bsg could be a key component coupling organization of the plasma membrane and cytoplasmic vesicular compartments. Consistent with such a role, we have observed defects in "plasma membrane versus internal membrane" sorting of presynaptic transmembrane components (for internal accumulation of HRP epitopes, see Fig. 7, D and E; not depicted). We thus propose that Bsg may be part of a transsynaptic complex surrounding active zones and involved in the coordinated development of pre- and postsynaptic membranes, as well as in the functional coupling of plasma membrane and cytoplasmic vesicles. Notably, Bsg recently has been identified within synaptic vesicle preparations (Takamori et al., 2006).

Bsg might act directly, or through interaction with transmembrane and cytoplasmic partners. Consistent with this latter hypothesis, we have shown that conserved amino acids found in the cytoplasmic tail of Bsg are crucial for the function of the protein in vivo and that they may thus mediate transduction of a signal toward the cell cytoplasm and/or interaction with the cortical cytoskeleton (see the following section).

### Basigin and the actin cytoskeleton

The F-actin/Spectrin cytoskeleton underlying pre- and postsynaptic membranes seems essential for different aspects of synaptic terminal growth and plasticity, including terminal expansion, organization of presynaptic vesicle pools, and postsynaptic receptor clustering (Dillon and Goda, 2005; Pielage et al., 2006; Ruiz-Canada and Budnik, 2006). Here, we have shown that Bsg modulates the organization of the presynaptic actin cytoskeleton, as revealed by the presence of ectopic aggregates of F-actin and actin-associated proteins within the lumen of *bsg* synaptic boutons. Although we could not detect any obvious alterations of the postsynaptic actin cytoskeleton, which is intermingled with the dense membraneous network of the SSR, it is nonetheless possible that Bsg also regulates this cytoskeleton. Our observations further support previous reports showing that Bsg colocalizes with the actin cytoskeleton specifically at cell–cell contacts and that expression of Bsg in cultured cells results in reorganization of the F-actin network and consequent formation of lamellipodia (Schlosshauer et al., 1995; Curtin et al., 2005).

At the NMJ, Bsg may modulate actin cytoskeleton organization indirectly, by interacting with integrin subunits at the plasma membrane. Indeed, mammalian Bsg has been found in

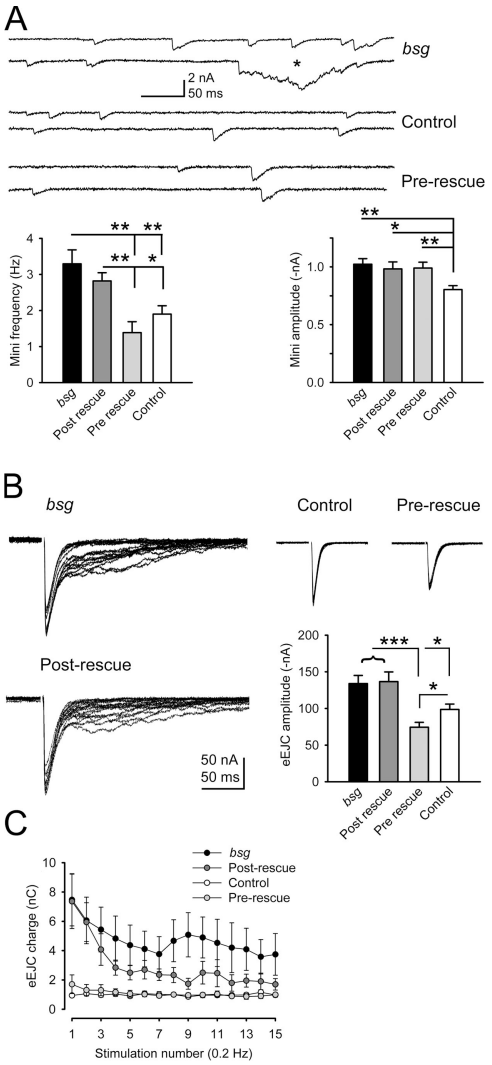


Figure 9. **Presynaptic loss of Bsg provokes asynchronous vesicle release.** (A) Representative traces and quantification of mini frequency and amplitude in *bsg* mutants and rescued animals. *, $P \leq 0.05$; **, $P \leq 0.01$. (B) Example traces of eEJCs after 15 stimuli at 0.2 Hz and mean amplitudes. *, $P \leq 0.05$; **, $P \leq 0.01$;***, $P \leq 0.001$. (C) Presynaptic loss of Bsg leads to an increased and atypically delayed release of vesicles, reflected by the larger charge carried by eEJCs of both *bsg* mutants and postsynaptic rescues. Precise genotypes are as follows: Basigin, *Df/bsg*$^{6293}$; control, *elav*-Gal4/Y; prerescue, *elav*-Gal4/Y; *Df/bsg*$^{6293}$; UAS-*bsg*/+; postrescue, *Df/bsg*$^{6293}$; UAS-*bsg*/*mhc*-Gal4.

a complex with β1-integrin (Berditchevski et al., 1997; Xu and Hemler, 2005), and both α- and β-integrin subunits colocalize with *D. melanogaster* Bsg at larval NMJs (Beumer et al., 1999; unpublished data). Furthermore, although we have not detected a genetic interaction between *bsg* and *myspheroid* (*mys*, which encodes the main *D. melanogaster* β-integrin subunit) during larval NMJ development, we identified several *mys* missense mutations displaying a junction undergrowth phenotype very similar to that of *bsg* mutants (Jannuzi et al., 2004; unpublished data). Another attractive hypothesis is that Bsg, through its juxtamembrane cytoplasmic motif, recruits Spectrin or other actin-associated proteins and thereby directly participates in organizing a cortical actin network. Interestingly, different members of the FERM domain protein family have been shown to link cell surface glycoproteins and the actin cytoskeleton by directly binding to both the intracellular region of transmembrane proteins and to actin or Spectrin (Tsukita and Yonemura, 1999; Bretscher et al., 2002). In particular, Moesin directly interacts with the intracytoplasmic domains of mammalian CD43, CD44, and intercellular adhesion molecule 2, through a positively charged amino acid cluster found in the juxtamembrane region of these proteins (Legg and Isacke, 1998; Yonemura et al., 1998). The striking conservation and functional importance of the KRR juxtamembrane motif of Bsg suggests that such cytoplasmic proteins may physically link cell-surface Bsg to the underlying F-actin network and mediate organization of cortical domains at the NMJ.

### Basigin controls synaptic vesicle release

Down-regulation of *bsg* at *D. melanogaster* NMJ terminals causes a dramatic increase in transmitter release, which, to our knowledge, is unique among Ig CAM mutants. This phenotype corresponds to a specific presynaptic function of Bsg and may be explained by (1) an alteration of the excitability of the synaptic terminal or (2) an altered definition of the different functional synaptic vesicle pools.

Mammalian Bsg has been shown to promote translocation of transporter proteins to the plasma membrane, as well as regulate the activity of multiprotein transmembrane complexes (Kirk et al., 2000; Zhou et al., 2005). At the *D. melanogaster* NMJ, Bsg may thus be required for the proper distribution and/or clustering of ion channels regulating $Ca^{2+}$ dynamics. In this context, it was recently demonstrated that the presynaptic scaffolding protein BRP is required for the clustering of $Ca^{2+}$ channels and for their spatial coupling with synaptic vesicles at the *D. melanogaster* active zone. This process appears to be required for the rapid evoked component of synaptic vesicle release but not for spontaneous release (Kittel et al., 2006). Therefore, both the additional spontaneous and delayed evoked component of transmitter release in *bsg* mutants might correspond to the fusion of vesicles lacking a tight association with $Ca^{2+}$ channels. An elevated contribution of asynchronous release has also been reported to occur naturally at particular synapses of the mammalian central nervous system and is thought to reflect long-lasting $Ca^{2+}$ transients and a loose coupling between $Ca^{2+}$ sources and vesicles (Hefft and Jonas, 2005). It is thus conceivable that down-regulation of Bsg alters $Ca^{2+}$ dynamics, leading to an abnormal recruitment of vesicles distant from $Ca^{2+}$ sources.

Alternatively, the observed transmitter release phenotype may not be associated with an alteration of $Ca^{2+}$ signals, but rather reflects a role of Bsg in organizing synaptic vesicle populations. It has been suggested that synaptic vesicles are organized into functionally distinct pools (readily releasable pool, recycling pool, and reserve pool) with specific recycling and mobilization properties (Rizzoli and Betz, 2004, 2005). Here, we have shown that down-regulation of *bsg* leads to an abnormal distribution of vesicles in resting terminals (Fig. 8), as well as an aberrant trafficking of vesicles to the center of boutons (where reserve pool vesicles are thought to reside) under conditions where synaptic vesicle recycling is normally restricted

to the periphery (and to the recycling pool; Fig. S3, C and D). These data suggest that the definition of different synaptic vesicle populations may be altered in *bsg* mutants, which in turn may explain the observed defects in precise recruitment and release of vesicles. This is of particular interest given that mammalian Bsg has been suggested to physically associate with synaptic vesicles (Takamori et al., 2006). Additionally, presynaptic actin filaments have been proposed to provide a physical barrier impeding vesicle dispersion and, in particular, to regulate the availability of the reserve pool (Dillon and Goda, 2005). They have also been suggested to participate in a mechanism restraining fusion of synaptic vesicles in cultured hippocampal neurons (Morales et al., 2000). An attractive possibility is therefore that Bsg controls synaptic vesicle organization and retention through its effect on the cortical actin cytoskeleton.

## Materials and methods

**Screening procedure**

In brief, +/Y; pBac[3xP3-DsRed; GFPexon]/+; pHer[3xP3-ECFP; α-tub-piggyBacK10]/+ jumpstarter males, carrying the protein-trap transposon and a source of *piggyBac* transposase (Horn et al., 2003), but not expressing any detectable GFP, were used to mobilize the GFP cassette and create new insertions. Jumpstarter males were crossed en masse with *w* virgins, and embryos were collected at 25°C on apple juice plates for either 5 h (for late embryo sorts) or overnight (for L1 sorts). They were then aged to stage 16–17 embryos and L1 larvae, respectively. Dechorionated embryos or L1 larvae were sorted using an embryo sorter (COPAS Select 500; Union Biometrica), following a procedure adapted from Furlong et al. (2001). Sorted larvae were then manually rescreened at later stages using a stereomicroscope (MZFLIII; Leica) equipped with standard GFP filters. About 350 $GFP^+$ individuals from a total of ~1.5 million animals sorted (1 million sorted as young larvae and 0.5 million sorted as late embryos) were selected, which roughly corresponds to a frequency of $GFP^+$ event recovery of 1/2,000–2,500 (estimated after taking into account the percentage of lethality).

Emerging $GFP^+$ individuals were then crossed individually to *w* flies to establish independent lines. Third instar larvae from each line were dissected, briefly fixed (5 min in 4% PFA), and washed several times in PBT. Fillet preparations were examined for GFP distribution using an epifluorescence microscope. For lines of interest, the position of the inserted protein-trap transposon was determined by sequencing of the flanking genomic regions using the inverse PCR protocol described by Horn et al. (2003). The exact positions (in the genomic scaffold AE003619) of the three *piggyBac* protein-trap insertions described are the following: 271285 (line 05.02), 277305 (line 91.03), and 278932 (line 79.13). Although two of these insertions (05.02 and 79.13) are homozygous viable, with homozygous larvae showing a rather normal NMJ morphology, one insertion is homozygous lethal (91.03). Given that the three insertions are located in the same intron, and thus generate the same fusion protein, this lethality is not associated with production of the chimeric protein.

**Fly stocks and transgenes**

The NP6293, l(2)SH1217, and l(2)k13638 insertions, and the deficiency covering *bsg* locus (*Df[2L]Exel7034*), were obtained from the Kyoto, Szeged, and Bloomington stock centers, respectively. NP6293 and l(2)1217 lie at position 267161 and 267380 of 2L, respectively. The NP6293 chromosome contains a single *P* element insertion (as verified by inverse PCR), but contains an additional mutation outside of the region covered by *Df(2L)Exel7034*, as indicated by the fact that both NP6293 and $NP6293^{pr.ex.}$ homozygous animals never reach larval stages, whereas a good number of NP6293/*Df(2L)Exel7034* larvae survive until third larval instar. For precise excision of NP6293, NP6293/CyO; Δ2-3, Sb/+ males were individually crossed to If/CyO females. A single w− CyO male per vial was then selected among the progeny and crossed to If/CyO virgin females to establish a stock. Excisions were then evaluated at the molecular level, by PCR amplification and sequencing of genomic DNA of hemizygous larvae. *mhc*-Gal4, $elav^{C155}$-Gal4, *tub*-Gal4, UAS-syt-EGFP, UAS-GMA stocks were obtained from the Bloomington stock center. All crosses were reared at 25°C.

The UAS-*bsg* transgene was generated by insertion of a 2.7-kb EcoRI–XhoI fragment obtained by double digestion of the DGC clone LD19437 into an EcoRI–XhoI digested pCasper3 vector. The following procedure was used to construct GFP-tagged full-length and mutated Bsg variants in which GFP insertion mimics that generated upon insertion of the protein-trap transposon. Total RNA was isolated from *bsg* protein-trap larval body wall preparations by standard Trizol extraction and used for reverse transcription with Superscript II RT (Invitrogen) and oligo dT primers. Reverse transcription products were then subjected to further PCR and cloned into a pENTR/DTOPO vector (Gateway technology; Invitrogen). One of the full-length GFP-tagged Bsg clones obtained was used as a template to construct the other Bsg variants. Insertion of the different Bsg-tagged proteins into pUASt vector was achieved through a LR recombination reaction (Gateway technology; Invitrogen) using pTW as a destination vector (Drosophila Gateway Vector Collection; http://www.ciwemb.edu/labs/murphy/Gateway%20vectors.html). Lines expressing similar levels of GFP-tagged mutant proteins were used for the rescue experiments described in Fig. 5 (not depicted).

**Immunocytochemistry**

Dissections and immunostainings were performed as described by Qin et al. (2005), using the following antibodies: rabbit anti-GFP (1:1,000; Invitrogen), mouse anti-Dlg (1:1,000; Developmental Study Hybridoma Bank [DSHB]), mouse anti-CSP (1:40; a gift from E. Buchner, Theodor-Boveri-Institute, Würzburg, Germany), mouse NC82 anti-BRP (1:50; [Wagh et al., 2006]), mouse anti-Synapsin (1:20; a gift from E. Buchner), rabbit anti–α-Spectrin (1:100; a gift from R. Dubreuil, University of Illinois at Chicago, Chicago, IL), mouse anti–α-Spectrin (1:50; clone 3A9; DSHB), mouse anti-Futsch (1:50; clone 22C10; DSHB), guinea pig anti-Wasp (1:400; Bogdan et al., 2005), FITC- and Cy5-conjugated anti-HRP (Cappel and Jackson ImmunoResearch Laboratories, respectively). Alexa Fluor 488 (Invitrogen), Cy3 or Cy5 (Jackson ImmunoResearch Laboratories) conjugated secondary antibodies were used at a 1:500 dilution. Unless specified, confocal pictures are those of muscles 6/7 NMJs (segments A2–A4) and were taken with a microscope (DMR-E; Leica) equipped with a scan head (TCS SP2 AOBS; Leica) and an oil-immersion 63× 1.4 NA objective.

For bouton number quantifications, type $I_b$ boutons of muscles 6/7 on segment A2 were counted using anti-CSP and anti-HRP double stainings. Muscles were photographed at 20× magnification and then traced and measured using ImageJ. The normalized bouton number was calculated by the dividing bouton number by the muscle surface area (data are expressed as a percentage of the *w* controls in each experiment). Although $Df/bsg^{6293}$ larvae exhibited muscles of a rather normal size, $Df/bsg^{1217}$ larvae have smaller muscles. Larvae with extremely thin muscles were excluded from the quantification of normalized bouton numbers. For bouton surface area quantification, confocal pictures of muscle 4 NMJs (segment A2) stained with anti-HRP antibodies were taken with a 63× magnification. Sections along the z axis were projected, and individual type $I_b$ boutons were then manually traced and measured using ImageJ. For measurement of $BRP^+$ puncta density, sections of NMJ 6/7 branches were projected along the z axis, and the density was calculated as the ratio between the total number of puncta and the projected surface of the branch (using Image J).

**Generation of antibody and Western blotting**

Rat polyclonal anti-Bsg antibodies were raised against an N-terminal synthetic peptide (QSLDKLVPNYD) obtained from Thermo Scientific. Crude serum was used at a 1:200 dilution for immunostainings and at a 1:1,500 dilution for Western blot analysis. Insertion of GFP within the epitope used to generate anti-Bsg antibodies probably explains the lower signal observed for tagged versus untagged Bsg proteins (Fig. 1 C). The highest molecular weight isoform detected in total larval extracts is not detected in body wall extracts (Fig. 3 C) and might correspond to a glycosylated form, as described for mammalian Bsg. The following antibodies were used for Western blot analysis: rabbit anti-GFP (1:500 [Santa Cruz Biotechnology, Inc.] or 1:2,500 [Torrey Pines]) and HRP-conjugated anti–mouse, –rat, or –rabbit (1:2,000; GE Healthcare) antibodies.

**Cell aggregation assay**

3 ml of a $10^6$ cells/ml culture of met-Gal4–expressing S2 cells were plated and transfected the next day with 3.5 μg of either UAS-Golgi-GFP or UAS-GFP-Bsg. After overnight recovery, cells were induced for 30 h with 0.7 mM $CuSO_4$, shortly centrifuged, and resuspended at $2 \times 10^6$ cells/ml in *D. melanogaster* SFM medium (Invitrogen) containing 18 mM L-Glutamine, 50 U/ml penicillin, and 50 g/ml streptomycin and puromycin. 1 ml of each suspension was placed in a 2-ml tube and shaken for 1 h at room

temperature. Aliquots were spotted on slides and examined using Nomarski optics and epifluorescence microscopy.

**Transmission EM**

Transmission micrographs were obtained from dissected preparations of third instar larvae (NMJ 6/7 and 12/13, segment A2/A3), as described by Wagh et al. (2006). All measurements were done using ImageJ. The data are reported as mean ± SEM, and where included, p-values denote the significance according to the Mann-Whitney Rank Sum test. Measurement of synaptic vesicle diameter was performed on populations of vesicles found within a radius of 300 nm around active zone T-bars.

**Electrophysiology**

Two-electrode voltage clamp recordings were obtained at 22°C from VLM 6 in segments A2 and A3, of late third instar larvae, essentially as previously described (Kittel et al., 2006). The composition of the extracellular haemolymph-like saline (HL-3) was as follows: 70 mM NaCl, 5 mM KCl, 20 mM $MgCl_2$, 10 mM $NaHCO_3$, 5 mM trehalose, 115 mM sucrose, 5 mM Hepes, and 1 mM $CaCl_2$, pH adjusted to 7.2. Minis (voltage clamp at −80 mV) and eEJCs (voltage clamp at −60 mV) were recorded with intracellular microelectrodes filled with 3 M KCl to give final resistances of 8–21 MΩ. The data are reported as mean ± SEM. *n* indicates the number of cells examined, and where included, p-values denote the significance according to the Mann-Whitney Rank Sum test. In the figures, the level of significance is marked with asterisks: *, $P \leq 0.05$; **, $P \leq 0.01$; ***, $P \leq 0.001$. The quantal content was roughly estimated as the ratio between the mean charge transferred per action potential and the mean charge carried by single minis (see Tables S2 for raw values).

**FM1-43 labeling assays**

The procedure used for FM1-43 labeling was adapted from Kuromi and Kidokoro (1998). For quantification of FM1-43 distribution upon loading (Fig. S3 C), fillets of third instar larvae were dissected in $Ca^{2+}$-free saline (130 mM NaCl, 36 mM sucrose, 5 mM KCl, 4 mM $MgCl_2$, and 5 mM Hepes) and incubated for 6 min with high-$K^+$ saline (45 mM NaCl, 36 mM sucrose, 90 mM KCl, 2 mM $MgCl_2$, 2 mM $CaCl_2$, 5 mM Hepes, and 0.5 mM EGTA) containing 7 μl/ml ($\sim 10^{-5}$ mol.$l^{-1}$) of a 1 μg/μl FM1-43X solution (Invitrogen). Fillets were then briefly washed two times in $Ca^{2+}$-free saline, fixed for 5 min in 4% formaldehyde, and washed quickly before being mounting on a slide. FM1-43 fluorescence was imaged right after using a confocal microscope (SP2; Leica).

For analysis of FM1-43 loading and unloading, fillets of third instar larvae were dissected in $Ca^{2+}$-free saline, transferred into a microscope chamber, and incubated for 5 min with high-$K^+$ saline containing 6 μl/ml ($\sim 10^{-5}$ mol.$l^{-1}$) of FM1-43 dye (Invitrogen). Preparations were then briefly rinsed three times with $Ca^{2+}$-free saline, further washed (once for 5 min and once for 10 min) with $Ca^{2+}$-free saline, and imaged using confocal microscopy and a 40× immersion objective ("after loading" pictures). We could not quantify the amount of FM1-43 dye loaded after the first part of the procedure, as *bsg* muscles contract longer than wild-type muscles upon transfer to $Ca^{2+}$-free saline, and thus start unloading part of the dye. We also noticed that contractions provoked by the high-$K^+$ solution are weaker in muscle 4 than in muscles 6/7, and therefore imaged exclusively muscle 4 NMJs. For unloading, two consecutive rounds of high-$K^+$ saline stimulation (1 min each), separated by washes with $Ca^{2+}$-free saline (three times for 5 min), were then applied in the absence of any dye. Junctions were imaged after further washing ("after unloading" pictures), using the same confocal settings as for the "after loading" pictures.

**Online supplemental material**

Fig. S1 shows second instar larvae NMJ morphology and cell–cell aggregation assays performed with Bsg variants. Fig. S2 shows the distribution of pre- and postsynaptic markers in *bsg* larvae. Fig. S3 shows the localization of synaptic vesicle–associated proteins (serial confocal sections), the distribution of mini amplitudes, and FM1-43 labeling assays. Table S1 shows raw bouton number and size in mutant and rescued contexts. Table S2 shows recorded electrophysiological properties of mutant and rescued larvae. Online supplemental material is available at http://www.jcb.org/cgi/content/full/jcb.200701111/DC1.

We thank the laboratories that made their fly strains and reagents available, as well as the Developmental Studies Hybridoma Bank at the University of Iowa for antibodies. We are very grateful to R. Ventzky, A. Cyrklaff, and S. Lopez de Quinto for their help during the screen; A.M. Voie for fly injections; T. Vaccari for the GFP-Golgi control construct; and laboratory members for help and discussion.

F. Besse was supported by fellowships from the Federation of European Biochemical Societies and the Human Frontier Science Program Organization.

Submitted: 19 January 2007
Accepted: 5 May 2007

## References

Berditchevski, F., S. Chang, J. Bodorova, and M.E. Hemler. 1997. Generation of monoclonal antibodies to integrin-associated proteins. Evidence that alpha3beta1 complexes with EMMPRIN/basigin/OX47/M6. *J. Biol. Chem.* 272:29174–29180.

Beumer, K.J., J. Rohrbough, A. Prokop, and K. Broadie. 1999. A role for PS integrins in morphological growth and synaptic function at the postembryonic neuromuscular junction of *Drosophila*. *Development.* 126:5833–5846.

Bogdan, S., R. Stephan, C. Lobke, A. Mertens, and C. Klambt. 2005. Abi activates WASP to promote sensory organ development. *Nat. Cell Biol.* 7:977–984.

Bretscher, A., K. Edwards, and R.G. Fehon. 2002. ERM proteins and merlin: integrators at the cell cortex. *Nat. Rev. Mol. Cell Biol.* 3:586–599.

Collins, M.O., H. Husi, L. Yu, J.M. Brandon, C.N. Anderson, W.P. Blackstock, J.S. Choudhary, and S.G. Grant. 2006. Molecular characterization and comparison of the components and multiprotein complexes in the postsynaptic proteome. *J. Neurochem.* 97(Suppl. 1):16–23.

Curtin, K.D., I.A. Meinertzhagen, and R.J. Wyman. 2005. Basigin (EMMPRIN/CD147) interacts with integrin to affect cellular architecture. *J. Cell Sci.* 118:2649–2660.

Dillon, C., and Y. Goda. 2005. The actin cytoskeleton: integrating form and function at the synapse. *Annu. Rev. Neurosci.* 28:25–55.

Dutta, D., J.W. Bloor, M. Ruiz-Gomez, K. VijayRaghavan, and D.P. Kiehart. 2002. Real-time imaging of morphogenetic movements in *Drosophila* using Gal4-UAS-driven expression of GFP fused to the actin-binding domain of moesin. *Genesis.* 34:146–151.

Fadool, J.M., and P.J. Linser. 1993. 5A11 antigen is a cell recognition molecule which is involved in neuronal-glial interactions in avian neural retina. *Dev. Dyn.* 196:252–262.

Fan, Q.W., S. Yuasa, N. Kuno, T. Senda, M. Kobayashi, T. Muramatsu, and K. Kadomatsu. 1998. Expression of basigin, a member of the immunoglobulin superfamily, in the mouse central nervous system. *Neurosci. Res.* 30:53–63.

Furlong, E.E., D. Profitt, and M.P. Scott. 2001. Automated sorting of live transgenic embryos. *Nat. Biotechnol.* 19:153–156.

Guo, H., S. Zucker, M.K. Gordon, B.P. Toole, and C. Biswas. 1997. Stimulation of matrix metalloproteinase production by recombinant extracellular matrix metalloproteinase inducer from transfected Chinese hamster ovary cells. *J. Biol. Chem.* 272:24–27.

Hefft, S., and P. Jonas. 2005. Asynchronous GABA release generates long-lasting inhibition at a hippocampal interneuron-principal neuron synapse. *Nat. Neurosci.* 8:1319–1328.

Horn, C., N. Offen, S. Nystedt, U. Hacker, and E.A. Wimmer. 2003. piggyBac-based insertional mutagenesis and enhancer detection as a tool for functional insect genomics. *Genetics.* 163:647–661.

Huang, R.P., M. Ozawa, K. Kadomatsu, and T. Muramatsu. 1993. Embigin, a member of the immunoglobulin superfamily expressed in embryonic cells, enhances cell-substratum adhesion. *Dev. Biol.* 155:307–314.

Jannuzi, A.L., T.A. Bunch, R.F. West, and D.L. Brower. 2004. Identification of integrin beta subunit mutations that alter heterodimer function in situ. *Mol. Biol. Cell.* 15:3829–3840.

Kasinrerk, W., N. Tokrasinwit, and P. Phunpae. 1999. CD147 monoclonal antibodies induce homotypic cell aggregation of monocytic cell line U937 via LFA-1/ICAM-1 pathway. *Immunology.* 96:184–192.

Kirk, P., M.C. Wilson, C. Heddle, M.H. Brown, A.N. Barclay, and A.P. Halestrap. 2000. CD147 is tightly associated with lactate transporters MCT1 and MCT4 and facilitates their cell surface expression. *EMBO J.* 19:3896–3904.

Kittel, R.J., C. Wichmann, T.M. Rasse, W. Fouquet, M. Schmidt, A. Schmid, D.A. Wagh, C. Pawlu, R.R. Kellner, K.I. Willig, et al. 2006. Bruchpilot promotes active zone assembly, $Ca^{2+}$ channel clustering, and vesicle release. *Science.* 312:1051–1054.

Koh, T.W., P. Verstreken, and H.J. Bellen. 2004. Dap160/intersectin acts as a stabilizing scaffold required for synaptic development and vesicle endocytosis. *Neuron.* 43:193–205.

Kuromi, H., and Y. Kidokoro. 1998. Two distinct pools of synaptic vesicles in single presynaptic boutons in a temperature-sensitive *Drosophila* mutant, *shibire*. *Neuron.* 20:917–925.

Lahey, T., M. Gorczyca, X.X. Jia, and V. Budnik. 1994. The *Drosophila* tumor suppressor gene *dlg* is required for normal synaptic bouton structure. *Neuron.* 13:823–835.

Legg, J.W., and C.M. Isacke. 1998. Identification and functional analysis of the ezrin-binding site in the hyaluronan receptor, CD44. *Curr. Biol.* 8:705–708.

Marie, B., S.T. Sweeney, K.E. Poskanzer, J. Roos, R.B. Kelly, and G.W. Davis. 2004. Dap160/intersectin scaffolds the periactive zone to achieve high-fidelity endocytosis and normal synaptic growth. *Neuron.* 43:207–219.

Morales, M., M.A. Colicos, and Y. Goda. 2000. Actin-dependent regulation of neurotransmitter release at central synapses. *Neuron.* 27:539–550.

Morin, X., R. Daneman, M. Zavortink, and W. Chia. 2001. A protein trap strategy to detect GFP-tagged proteins expressed from their endogenous loci in *Drosophila*. *Proc. Natl. Acad. Sci. USA.* 98:15050–15055.

Muramatsu, T., and T. Miyauchi. 2003. Basigin (CD147): a multifunctional transmembrane protein involved in reproduction, neural function, inflammation and tumor invasion. *Histol. Histopathol.* 18:981–987.

Nabeshima, K., H. Iwasaki, K. Koga, H. Hojo, J. Suzumiya, and M. Kikuchi. 2006. Emmprin (basigin/CD147): matrix metalloproteinase modulator and multifunctional cell recognition molecule that plays a critical role in cancer progression. *Pathol. Int.* 56:359–367.

Naruhashi, K., K. Kadomatsu, T. Igakura, Q.W. Fan, N. Kuno, H. Muramatsu, T. Miyauchi, T. Hasegawa, A. Itoh, T. Muramatsu, and T. Nabeshima. 1997. Abnormalities of sensory and memory functions in mice lacking *Bsg* gene. *Biochem. Biophys. Res. Commun.* 236:733–737.

Pielage, J., R.D. Fetter, and G.W. Davis. 2005. Presynaptic spectrin is essential for synapse stabilization. *Curr. Biol.* 15:918–928.

Pielage, J., R.D. Fetter, and G.W. Davis. 2006. A postsynaptic Spectrin scaffold defines active zone size, spacing, and efficacy at the *Drosophila* neuromuscular junction. *J. Cell Biol.* 175:491–503.

Polo-Parada, L., C.M. Bose, and L.T. Landmesser. 2001. Alterations in transmission, vesicle dynamics, and transmitter release machinery at NCAM-deficient neuromuscular junctions. *Neuron.* 32:815–828.

Ponta, H., L. Sherman, and P.A. Herrlich. 2003. CD44: from adhesion molecules to signalling regulators. *Nat. Rev. Mol. Cell Biol.* 4:33–45.

Qin, G., T. Schwarz, R.J. Kittel, A. Schmid, T.M. Rasse, D. Kappei, E. Ponimaskin, M. Heckmann, and S.J. Sigrist. 2005. Four different subunits are essential for expressing the synaptic glutamate receptor at neuromuscular junctions of *Drosophila*. *J. Neurosci.* 25:3209–3218.

Rizzoli, S.O., and W.J. Betz. 2004. The structural organization of the readily releasable pool of synaptic vesicles. *Science.* 303:2037–2039.

Rizzoli, S.O., and W.J. Betz. 2005. Synaptic vesicle pools. *Nat. Rev. Neurosci.* 6:57–69.

Rougon, G., and O. Hobert. 2003. New insights into the diversity and function of neuronal immunoglobulin superfamily molecules. *Annu. Rev. Neurosci.* 26:207–238.

Ruiz-Canada, C., and V. Budnik. 2006. Synaptic cytoskeleton at the neuromuscular junction. *Int. Rev. Neurobiol.* 75:217–236.

Ruiz-Canada, C., J. Ashley, S. Moeckel-Cole, E. Drier, J. Yin, and V. Budnik. 2004. New synaptic bouton formation is disrupted by misregulation of microtubule stability in aPKC mutants. *Neuron.* 42:567–580.

Schlosshauer, B., H. Bauch, and R. Frank. 1995. Neurothelin: amino acid sequence, cell surface dynamics and actin colocalization. *Eur. J. Cell Biol.* 68:159–166.

Schuster, C.M., G.W. Davis, R.D. Fetter, and C.S. Goodman. 1996a. Genetic dissection of structural and functional components of synaptic plasticity. I. Fasciclin II controls synaptic stabilization and growth. *Neuron.* 17:641–654.

Schuster, C.M., G.W. Davis, R.D. Fetter, and C.S. Goodman. 1996b. Genetic dissection of structural and functional components of synaptic plasticity. II. Fasciclin II controls presynaptic structural plasticity. *Neuron.* 17:655–667.

Smalla, K.H., H. Matthies, K. Langnase, S. Shabir, T.M. Bockers, U. Wyneken, S. Staak, M. Krug, P.W. Beesley, and E.D. Gundelfinger. 2000. The synaptic glycoprotein neuroplastin is involved in long-term potentiation at hippocampal CA1 synapses. *Proc. Natl. Acad. Sci. USA.* 97:4327–4332.

Sone, M., E. Suzuki, M. Hoshino, D. Hou, H. Kuromi, M. Fukata, S. Kuroda, K. Kaibuchi, Y. Nabeshima, and C. Hama. 2000. Synaptic development is controlled in the periactive zones of *Drosophila* synapses. *Development.* 127:4157–4168.

Stewart, B.A., C.M. Schuster, C.S. Goodman, and H.L. Atwood. 1996. Homeostasis of synaptic transmission in *Drosophila* with genetically altered nerve terminal morphology. *J. Neurosci.* 16:3877–3886.

Sun, J., and M.E. Hemler. 2001. Regulation of MMP-1 and MMP-2 production through CD147/extracellular matrix metalloproteinase inducer interactions. *Cancer Res.* 61:2276–2281.

Takamori, S., M. Holt, K. Stenius, E.A. Lemke, M. Gronborg, D. Riedel, H. Urlaub, S. Schenck, B. Brugger, P. Ringler, et al. 2006. Molecular anatomy of a trafficking organelle. *Cell.* 127:831–846.

Tang, Y., M.T. Nakada, P. Rafferty, J. Laraio, F.L. McCabe, H. Millar, M. Cunningham, L.A. Snyder, P. Bugelski, and L. Yan. 2006. Regulation of vascular endothelial growth factor expression by EMMPRIN via the PI3K-Akt signaling pathway. *Mol. Cancer Res.* 4:371–377.

Toole, B.P. 2003. Emmprin (CD147), a cell surface regulator of matrix metalloproteinase production and function. *Curr. Top. Dev. Biol.* 54:371–389.

Tsukita, S., and S. Yonemura. 1999. Cortical actin organization: lessons from ERM (ezrin/radixin/moesin) proteins. *J. Biol. Chem.* 274:34507–34510.

Wagh, D.A., T.M. Rasse, E. Asan, A. Hofbauer, I. Schwenkert, H. Durrbeck, S. Buchner, M.C. Dabauvalle, M. Schmidt, G. Qin, et al. 2006. Bruchpilot, a protein with homology to ELKS/CAST, is required for structural integrity and function of synaptic active zones in *Drosophila*. *Neuron.* 49:833–844.

Wucherpfennig, T., M. Wilsch-Brauninger, and M. Gonzalez-Gaitan. 2003. Role of *Drosophila* Rab5 during endosomal trafficking at the synapse and evoked neurotransmitter release. *J. Cell Biol.* 161:609–624.

Xu, D., and M.E. Hemler. 2005. Metabolic activation-related CD147-CD98 complex. *Mol. Cell. Proteomics.* 4:1061–1071.

Yamagata, M., J.R. Sanes, and J.A. Weiner. 2003. Synaptic adhesion molecules. *Curr. Opin. Cell Biol.* 15:621–632.

Yonemura, S., M. Hirao, Y. Doi, N. Takahashi, T. Kondo, and S. Tsukita. 1998. Ezrin/radixin/moesin (ERM) proteins bind to a positively charged amino acid cluster in the juxta-membrane cytoplasmic domain of CD44, CD43, and ICAM-2. *J. Cell Biol.* 140:885–895.

Zhai, R.G., and H.J. Bellen. 2004. The architecture of the active zone in the presynaptic nerve terminal. *Physiology (Bethesda).* 19:262–270.

Zhou, S., H. Zhou, P.J. Walian, and B.K. Jap. 2005. CD147 is a regulatory subunit of the gamma-secretase complex in Alzheimer's disease amyloid beta-peptide production. *Proc. Natl. Acad. Sci. USA.* 102:7499–7504.